Biocatalyst activity in nonaqueous environments correlates with centisecond-range protein motions

Ross K. Eppler*, Elton P. Hudson*, Shannon D. Chase*, Jonathan S. Dordick‡, Jeffrey A. Reimer*, and Douglas S. Clark*§

*Department of Chemical Engineering, University of California, Berkeley, CA 94720; and ‡Department of Chemical and Biological Engineering, Rensselaer Polytechnic Institute, Troy, NY 12180

Edited by Alexander M. Klibanov, Massachusetts Institute of Technology, Cambridge, MA, and approved August 26, 2008 (received for review June 2, 2008)

Recent studies exploring the relationship between enzymatic catalysis and protein dynamics in the aqueous phase have yielded evidence that dynamics and enzyme activity are strongly correlated. Given that protein dynamics are significantly attenuated in organic solvents and that proteins exhibit a wide range of motions depending on the specific solvent environment, the nonaqueous milieu provides a unique opportunity to examine the role of protein dynamics in enzyme activity. Variable-temperature kinetic measurements, X-band electron spin resonance spectroscopy, ^{1}H NMR relaxation, and ^{19}F NMR spectroscopy experiments were performed on subtilisin Carlsberg colyophilized with several inorganic salts and suspended in organic solvents. The results indicate that salt activation induces a greater degree of transition-state flexibility, reflected by a more positive $\Delta\Delta S^{\dagger}$, for the more active biocatalyst preparations in organic solvents. In contrast, $\Delta\Delta H^{\dagger}$ was negligible regardless of salt type or salt content. Electron spin resonance spectroscopy and ^{1}H NMR relaxation measurements, including spin-lattice relaxation, spin-lattice relaxation in the rotating frame, and longitudinal magnetization exchange, revealed that the enzyme's turnover number (k_{cat}) was strongly correlated with protein motions in the centisecond time regime, weakly correlated with protein motions in the millisecond regime, and uncorrelated with protein motions on the piconanosecond timescale. In addition, ^{19}F chemical shift measurements and hyperfine tensor measurements of biocatalyst formulations inhibited with 4-fluorobenzenesulfonyl fluoride and 4-ethoxyfluorophosphinyl-oxy-TEMPO, respectively, suggest that enzyme activation was only weakly affected by changes in active-site polarity.

enzyme activation | enzyme dynamics | NMR spectroscopy | organic solvents | subtilisin Carlsberg

The direct coupling of protein dynamics to enzymatic catalysis is strongly supported by recent studies of enzymes in aqueous solution (1–3). These studies have revealed insights into the connection between enzyme activity and protein dynamics [e.g., conformation exchange in CypA (4), *Aquifex* Adk lid movement (5), Met-20 loop dynamics in DHFR (6), loop motions leading to conformational change in RNase A (7), and modulation of surface-glycosylated chymotrypsin structural dynamics and activity (8)], yet the relatively small range of enzyme activities accessible under aqueous conditions, without the use of protein modifications or alteration of the solvent, hinders thorough investigation of the central hypothesis that enzyme catalysis is intimately coupled to protein dynamics. One strategy for broadening the range of activities over which enzyme catalysis and protein dynamics can be studied concurrently is to employ nonaqueous or organic solvents. For example, a correlation between molecular dynamics, as evidenced by a reduced rate of amide H/D exchange, and biocatalyst activity has been observed for PEGylated subtilisin Carlsberg (SC) in 1,4-dioxane (9).

Nonaqueous biocatalysis was originally developed to take advantage of the exquisite selectivity and high catalytic rates of enzymes under ambient conditions while overcoming the limitations of aqueous solutions for practical applications (e.g., low substrate solubility, undesirable hydrolysis reactions, and low enzyme stability) (10–13). Unfortunately, native enzymes typically exhibit very low activities in nonnative solvent environments (10–13), although techniques have been developed to increase the activity of some enzymes to near aqueous levels (14–18). One such activation methodology, known as salt activation, is unique in that enzyme activity can be controlled over an unprecedented range (17, 18) (i.e., several orders of magnitude) without modifying the amino acid sequence, temperature, or bulk solvent environment. The wide range of activities accessible by salt-activated enzymes in the nonaqueous phase, coupled with the known attenuation of protein dynamics in nonaqueous media (19–21), provides a unique opportunity to rigorously examine the connection between enzyme activity and protein dynamics.

Salt activation of hydrolytic enzymes in organic solvents has been particularly well studied and partially optimized (with respect to water content, pH, lyophilization time, salt content, and physicochemical properties of the salt, e.g., Jones–Dole *B* coefficient) to yield near aqueous levels of activity (17, 18). The dramatic increase in catalytic rate is purportedly due to increased enzyme flexibility and/or increased active-site polarity (10, 11). Previous studies have produced a tunable activation methodology spanning several orders of magnitude for SC [e.g., k_{cat} (salt free) = 0.003 s^{-1} to k_{cat} (98% KCl) = 0.93 s^{-1}]. The present study seeks to specifically examine protein flexibility at different timescales in undissolved solid biocatalyst preparations and compare these results directly with biocatalyst turnover numbers and catalytic efficiencies. To elucidate the timescale of dynamics important to catalysis, as well as to distinguish active-site polarity versus dynamical activation effects, multinuclear NMR spectroscopy was used to measure enzyme motions within the salt-activated biocatalyst and probe polarity effects at the active site. Three time regimes were accessed by using ^{1}H NMR relaxometry: picosecond to tens of nanoseconds (via spin-lattice relaxation, T_{1H}), microsecond to millisecond (via spin-lattice relaxation in the rotating frame, $T_{1\rho H}$), and centisecond to second (via longitudinal magnetization exchange, T_{1zzH}) (22–24). Active-site polarity was investigated by monitoring the ^{19}F chemical shift of a fluorinated inhibitor located in the active site of SC. Finally, electron spin resonance (ESR) spectroscopy of active-site spin-labeled subtilisin was used to assess the influence of protein dynamics and active-site polarity on enzyme function in organic solvents.

Results and Discussion

Entropic and Enthalpic Contributions to Salt Activation. In an effort to illuminate the degree to which the mechanism(s) of salt activation is related to the enzyme's molecular dynamics versus increased active-site polarity (i.e., due mainly to entropic or enthalpic effects), variable temperature kinetic measurements were performed with

Author contributions: R.K.E., J.S.D., J.A.R., and D.S.C. designed research; R.K.E. and S.D.C. performed research; R.K.E., E.P.H., S.D.C., J.A.R., and D.S.C. analyzed data; and R.K.E., E.P.H., J.S.D., J.A.R., and D.S.C. wrote the paper.

The authors declare no conflict of interest.

This article is a PNAS Direct Submission.

§To whom correspondence should be addressed at: Department of Chemical Engineering, University of California, 201 Gilman Hall, Berkeley, CA 94720. E-mail: clark@berkeley.edu.

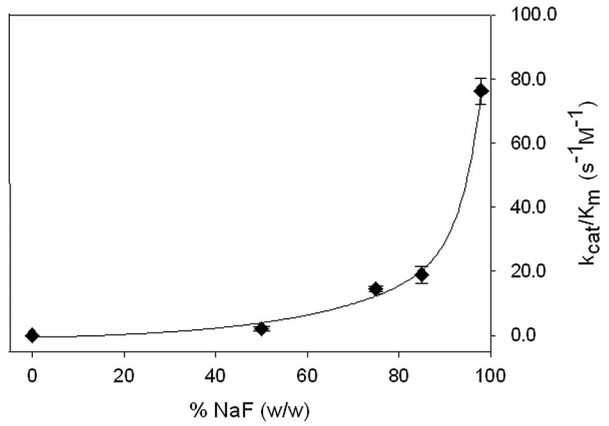

Fig. 1. Catalytic efficiency k_{cat}/K_m ($s^{-1}\cdot M^{-1}$) in hexane of SC biocatalysts containing different weight fractions of sodium fluoride.

SC colyophilized with several inorganic salts. Fig. 1 shows that biocatalyst activity increases nonlinearly as the percentage of salt increases, consistent with previous studies (17, 18, 25, 26). Factors proposed to account for this rise in activity include preferential hydration before freeze-drying and lyoprotectant effects (15, 27). Although structural preservation (e.g., lyoprotection) is observed with many sugars, salts, and polymeric excipients (28), the large activation (>3 orders of magnitude) achieved by salts in the organic phase is unique, suggesting that activation is not due solely to structural preservation.

If increased active-site polarity is the primary mechanism of activation, the salt-activated biocatalyst should reduce the activation enthalpy of reaction relative to the salt-free preparation (i.e., $\Delta\Delta H^{\dagger} < 0$, where $\Delta\Delta H^{\dagger} = \Delta H^{\dagger}_{\text{salt-activated}} - \Delta H^{\dagger}_{\text{salt-free}}$). In this interpretation, dynamic activation mechanisms should manifest as a gain in activation entropy (i.e., $\Delta\Delta S^{\dagger} > 0$) for salt-activated biocatalysis compared with salt-free reactions. $\Delta\Delta H^{\dagger}$ and $\Delta\Delta S^{\dagger}$ values for salt-activated preparations of subtilisin spanning a wide range of activities are shown in Fig. 2. Fig. 2*A* reveals that there is little or no observed increase in the enthalpic contribution to catalysis for the salt preparations relative to the salt-free preparation and that the observed increase in activity (k_{cat}/K_m) with percent NaF (Fig. 1) is due almost entirely to entropic effects. Greater activation entropy is consistent with greater degrees of conformational and/or motional freedom in the transition state, which we interpret as an increase in enzyme flexibility with higher salt content for reactions in both hexane and acetone.

Previously established activation trends based on the salt's chao/kosmotropicity (17, 18) reveal higher activation for salts containing chaotropic cations and kosmotropic anions. Although increases in enzyme dynamics have been proposed as a potential activation mechanism (10–12), a causative dynamics–activity relationship has not been rigorously validated. Fig. 2*B* shows a variable temperature kinetic analysis that reveals a large increase in $\Delta\Delta S^{\dagger}$ with $\Delta\delta$, the difference in Jones–Dole *B* coefficient between the anion and cation of the salt, as the salt type is altered from a nonoptimized preparation, 98% (wt/wt) NaCl (e.g., low activity), to the highly active 98% (wt/wt) $KHCO_3$ preparation. As observed for increasing weight percentage of NaF, salt activation is accompanied by a large $\Delta\Delta S^{\dagger}$ and a negligible $\Delta\Delta H^{\dagger}$, providing further evidence that the activation effect is primarily entropic/dynamic in nature.

Protein Dynamics Studied via ^{1}H NMR Relaxometry. Protein dynamics within the various biocatalysts were examined via solid-state ^{1}H NMR relaxation experiments. NMR signals due to residual water molecules associated with the biocatalyst samples were eliminated by lyophilizing all samples from D_2O. The measured relaxation values represent averages of proton motions on the enzyme. More detailed determination of local structure and dynamics, which have been reported for small, solid peptides and protein fragments (29–31), were precluded by the high molecular weight of subtilisin and the large homonuclear dipolar couplings associated with solid enzyme samples. However, prior evidence that bulk relaxation measurements in the solid state are a valid measure of enzyme dynamics has been provided previously where side-chain dynamics (measured via T_{1D}) of α-spectrin SH3 were found to be roughly constant regardless of their position in the amino acid sequence (29).

Three NMR relaxation experiments—namely, spin-lattice relaxation T_{1H}, spin-lattice relaxation in the rotating frame $T_{1\rho H}$, and longitudinal magnetization exchange T_{1zzH}—were used to probe molecular motions of subtilisin ensconced within the salt matrix of the biocatalyst. The NMR relaxation parameters (T_{1H}, $T_{1\rho H}$, and T_{1zzH}) represent a course-grain measurement of global protein

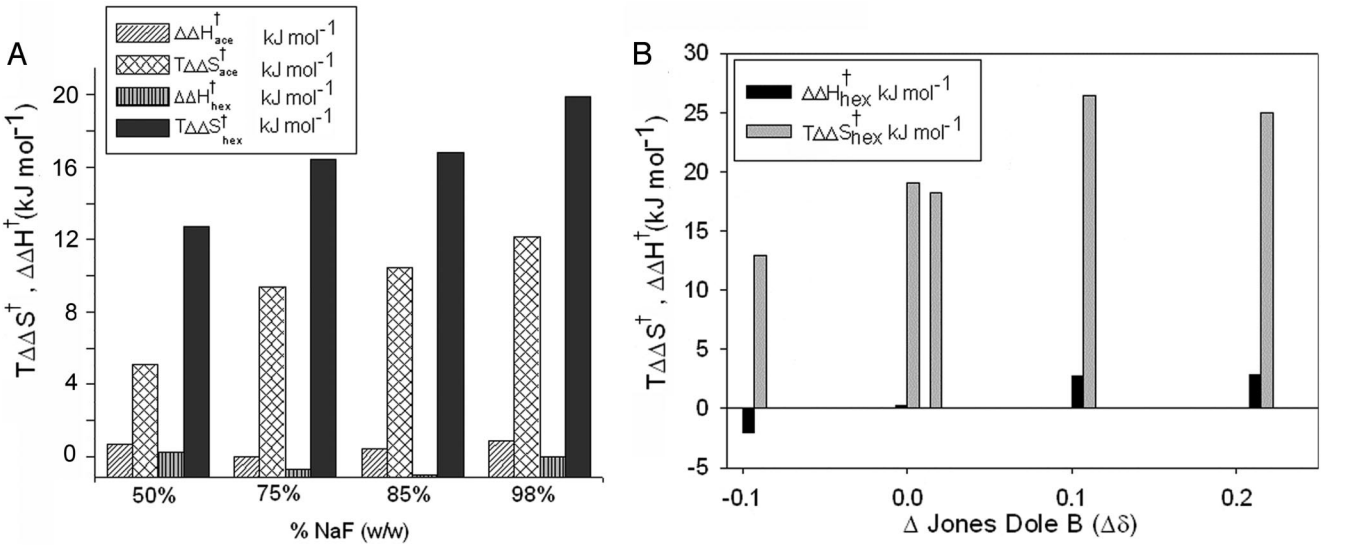

Fig. 2. Entropic ($T\Delta\Delta S^{\dagger}$, T = 303 K) and enthalpic ($\Delta\Delta H^{\dagger}$) contributions to catalysis for salt-activated SC. (*A*) NaF-activated SC in hexane and in acetone. (*B*) Ninety-eight percent (wt/wt) salt-activated SC in hexane as a function of Δ Jones–Dole *B* coefficient (20). Biocatalysts from left to right: 98% (wt/wt) NaCl, 98% (wt/wt) NaF, 98% (wt/wt) KCl, 98% (wt/wt) KF, and 98% (wt/wt) $KHCO_3$.

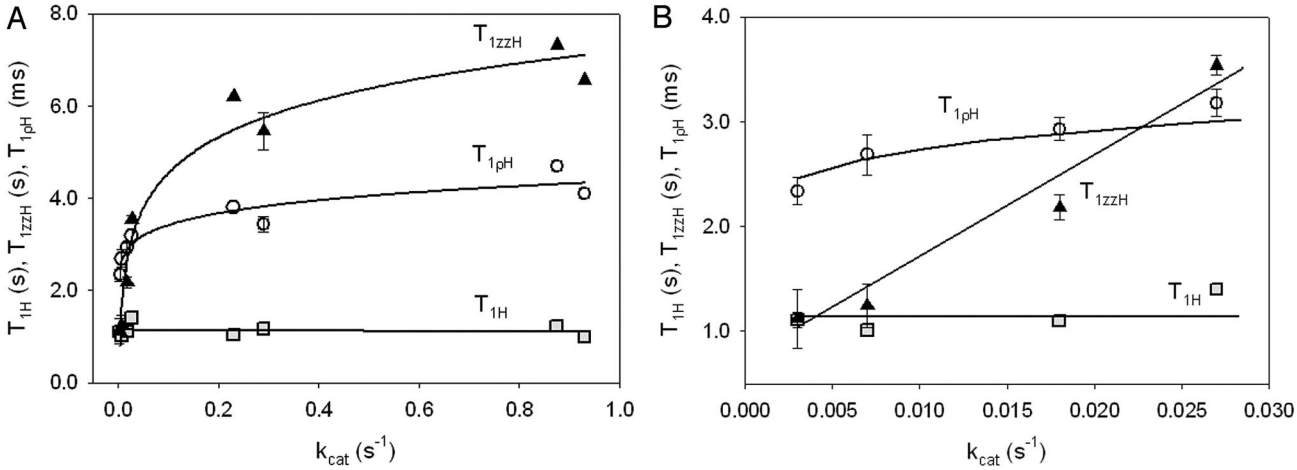

Fig. 3. ^{1}H MAS NMR relaxation studies of SC biocatalysts in hexane. (*A*) Total range of biocatalyst turnover numbers. (*B*) Expansion of low-activity regime: T_{1zzH} (filled triangles), $T_{1\rho H}$ (open circles), and T_{1H} (open squares). From left to right: salt-free, 50% (wt/wt) NaF, 75% (wt/wt) NaF, 85% (wt/wt) NaF, 98% (wt/wt) NaCl, 98% (wt/wt) NaF, 98% (wt/wt) KF, and 98% (wt/wt) KCl.

motion. Variable-field ^{1}H NMR relaxation experiments were performed at 200 MHz and 400 MHz to ensure that increases in the NMR relaxation parameters (T_{1H}, $T_{1\rho H}$, and T_{1zzH}) correspond with increases in molecular motion.

A previous deuterium NMR study revealed that salt-free SC contained a "loosely" bound nonexchanging water population (33% of the total water associated with the biocatalyst) (32). Further study of this water population indicated that the amount and motion of the residual water molecules associated with the biocatalyst correlated strongly with biocatalyst activity in an Arrhenius-like fashion, with residual water molecules in salt-activated biocatalysts exhibiting shorter correlation times for motion in the more active salt preparations (33). These water molecules exhibited correlation times in the picosecond-to-nanosecond time regime. Interestingly, in the present study no such correlations exist over the entire range of enzyme turnover for the proton relaxation parameter T_{1H}, which probes protein motions on the picosecond-to-nanosecond timescale, because there is little difference in the measured T_{1H} values (Fig. 3).

The data in Fig. 3*B* reveal that there is a slight increase in protein dynamics on the millisecond timescale, as reflected by $T_{1\rho H}$, in the activity regime from $k_{cat} = 0.003\ s^{-1}$ to $k_{cat} = 0.027\ s^{-1}$, and a larger increase on the centisecond timescale, as reflected by T_{1zzH}. Thus, initially a direct relationship exists between slow protein dynamics (T_{1zzH}) and enzyme turnover; however, as enzyme turnover increases beyond 0.23 s^{-1} protein dynamics on the centisecond timescale plateau dominate. This additional activation indicates that a secondary mechanism further increases the catalytic rate, albeit to a lesser degree (≈5-fold) compared with the dynamic mechanism (≈100-fold). Regardless of the nature of the secondary mechanism, that protein motion on the centisecond timescale is highly and intimately coupled to a catalytic event suggests that turnover is closely linked to protein dynamics and that the protein's dynamic freedom is strongly influenced by the presence of salt.

One possible explanation for the apparent incongruity between fast picosecond–nanosecond residual water dynamics and slow centisecond protein dynamics affecting biocatalyst activity is that the mobile water molecules exert a plasticizing effect on the protein, which manifests itself as an increase in protein motions on much slower timescales. It is noteworthy that numerous previous studies, including a recent study by our laboratory (33), provide evidence of correlations between fast solvent dynamics and molecular events evident on slower timescales [e.g., substrate dissociation in myoglobin (34); protein folding of cytochrome *c*, protein L, and human serum albumin (35, 36); and enzyme activity (37, 38)]. The intimate collusion between fast solvent dynamics and slow protein motion is referred to as solvent slaving and has been reported for many classes of proteins (39, 40).

Active-Site Polarity Measured via ^{19}F NMR. In an effort to directly measure the polarity in the enzyme's active site, Ser-221 of subtilisin was selectively tagged with 4-fluorobenzenesulfonyl fluoride (4-FBSF). Activity assays performed with 4-FBSF-inhibited biocatalyst in aqueous buffer, before lyophilization, and again in the organic phase after lyophilization (data not shown) guaranteed that the biocatalyst was inhibited by the sulfonyl species. ^{19}F chemical shifts were then measured for the salt-activated and salt-free ^{19}F-labeled catalysts. ^{19}F NMR spectra of 4-FBSF are highly sensitive to the dielectric constant of the solvent (Fig. 4). Thus, decreases in chemical shift relative to the salt-free preparation would provide evidence that the C–F bond is more polarized in the enzyme's active site. As shown in Fig. 5, the ^{19}F chemical shift is nearly unchanged as the turnover number of the enzyme increases from $k_{cat} = 0.003\ s^{-1}$ (salt-free) to $k_{cat} = 0.23\ s^{-1}$ (98% NaCl). The relatively small change in chemical shift suggests that there is little C–F bond polarization (i.e., little increase in active-site polarity). Despite these small changes in active-site polarity, the turnover number increases ≈100-fold in this region of salt activation. The nearly constant C–F bond polarization is consistent with the

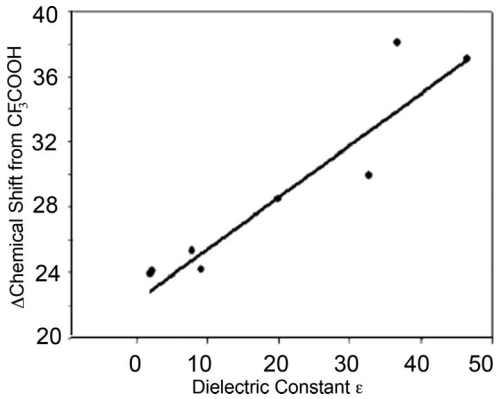

Fig. 4. ^{19}F NMR chemical shift measurements of 4-fluorobenzylsulfonyl chloride (4-FBSCl) in solvents of varying dielectric constant. Solvents, from left to right: *n*-hexane (ε = 1.9), isooctane (ε = 2.2), THF (ε = 7.8), CH_3Cl (ε = 9.1), acetone (ε = 20.7), methanol (ε = 32.7), DMF (ε = 36.7), and DMSO (ε = 46.5).

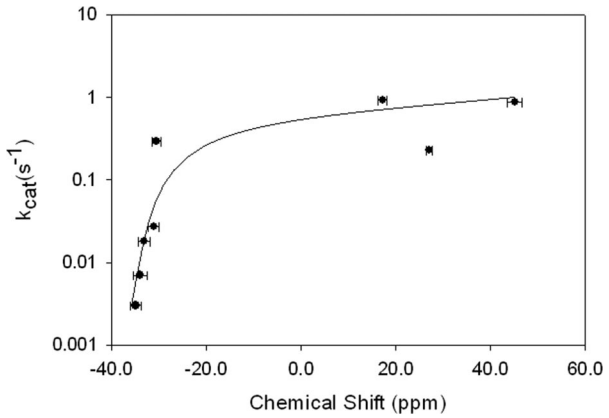

Fig. 5. ^{19}F NMR chemical shift measurements of 4-FBS-SC in hexane. From left to right: salt-free, 50% (wt/wt) NaF, 75% (wt/wt) NaF, 85% (wt/wt) NaF, 98% (wt/wt) NaCl, 98% (wt/wt) NaF, 98% (wt/wt) KF, and 98% (wt/wt) KCl.

negligible change in activation enthalpy shown in Fig. 2*A*, in which case activation appears to be related solely to molecular dynamics (i.e., a large increase in $\Delta\Delta S^{\ddagger}$ while $\Delta\Delta H^{\ddagger} \approx 0$).

Fig. 5 also shows a dramatic change in chemical shift ($\Delta CS \approx 90$ ppm) for the high range of biocatalyst activity, $k_{cat} = 0.23$–$0.93\ s^{-1}$. Such large shifts are not unprecedented for fluorobenzenes and have been attributed solely to increased polarization of the C–F bond (41). Interestingly, the large shifts observed in Fig. 5 accompany only a slight increase in k_{cat} (≈5-fold). Compared with the low activity range, where a 100-fold increase in activity occurs with little observable changes in ^{19}F chemical shift, these data indicate that active-site polarity is not the major factor in biocatalyst activation.

ESR Studies of Salt-Activated Biocatalysts. As an independent spectroscopic measure of global enzyme dynamics, ESR spectroscopy was used on a variety of salt-activated SC preparations. X-band ESR spectra were taken of the biocatalyst preparations selectively inhibited at the active-site serine (Ser-221) with 4-ethoxyfluorophosphinyl-oxy-TEMPO (ESL) in anhydrous hexane. The spectra presented in Fig. 6 reveal the existence of two spin-label populations. Control experiments performed with PMSF-inhibited SC ensured that the second population is not simply due to nonspecific binding of ESL.[¶] We surmise that these two populations are representative of two enzyme populations ensconced within the salt matrix, where one population exhibits faster spin-label dynamics. Presumably, the more dynamic population is more catalytically active because its increase in magnitude correlates with the increase in k_{cat}/K_m (Fig. 7). Whereas the proportion of faster population increases with increasing salt content, the overall dynamics of the spin label (τ_c) do not appear to change in an appreciable manner from sample to sample (Table 1).

The hyperfine splitting constant is a measure of the local electronic environment surrounding the nitroxide probe (42). Previous studies investigating the degree to which active-site polarity plays a role in immobilized chymotrypsin activity showed modest increases in A_0 relative to the freely suspended, less-active enzyme powder. These studies revealed that increased active-site polarity, which aids in the stabilization of chymotrypsin's polar transition state, was at least partly responsible for the observed 40-fold increase in activity (43). However, suspended chymotrypsin powders, which more closely resemble the physical and chemical make-up of the salt-activated biocatalysts, showed no correlation

[¶]If ESL binds to residues other than Ser-221, spectra of SC inhibited with PMSF and prepared in the same manner should include a signal indicative of nonspecifically bound ESL. These control experiments revealed no evidence of an ESR signal due to nonspecific binding of ESL (data not shown); thus, the spectra in Fig. 6 are of SC spin-labeled exclusively at Ser-221.

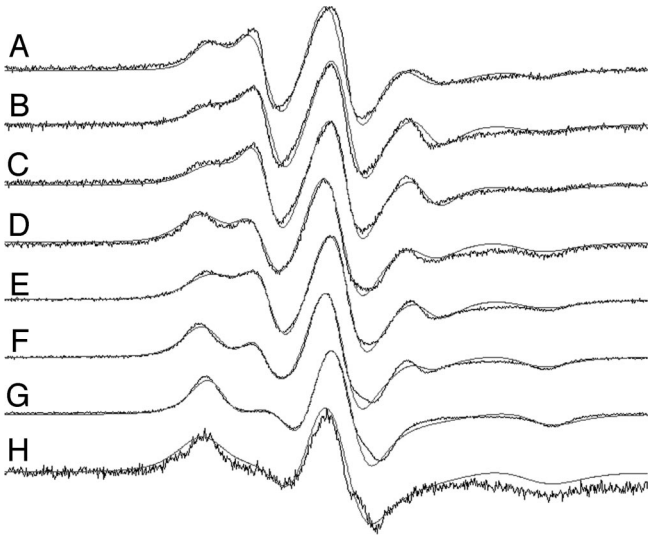

Fig. 6. Experimental (black) and simulated (gray) ESR spectra of salt-activated 4-FBS-SC in hexane: line A, 98% (wt/wt) KF; line B, 98% (wt/wt) KCl; line C, 98% (wt/wt) NaF; line D, 98% (wt/wt) NaCl; line E, 85% (wt/wt) NaF; line F, 75% (wt/wt) NaF; line G, 50% (wt/wt) NaF; line H, salt-free.

between activity and A_0. The hyperfine splitting parameter, A_0, of salt-activated SC does not exhibit significant changes as the activity of the biocatalyst increases from 0.092 $s^{-1}\cdot M^{-1}$ (salt-free) to 284 $s^{-1}\cdot M^{-1}$ (98% wt/wt KF). Thus, the independent spectroscopic data from ESR and NMR indicate that the role of increased active-site polarity to biocatalyst activation is small relative to protein dynamics.

Conclusions

In summary, ^{1}H NMR relaxation data in concert with variable temperature kinetic measurements revealed that salt activation is primarily entropic in nature regardless of the solvent and the composition of the excipient matrix. The spectroscopic and kinetic data indicate that salt activation of SC in organic solvents correlates with molecular dynamics of the enzyme, supporting a functional link between catalysis and protein motions. In addition, the motional timescale that is most influenced by the presence of salt is on the order of centiseconds. The existence of these slow molecular motions in the biocatalyst begs the question of how they affect the catalytic machinery of SC. A recent structural bioinformatics study employing coarse-grained elastic network modeling exhibited the pervasive overlap of large-scale dynamical fluctuations for many proteins in the aspartic dyad protease family (44). Similarly, a Gaussian network model was recently used to ascribe interdomain hinge-bending dynamics in α-chymotrypsin glycoconjugates to slower collective conformational dynamics, which were associated with hydrolysis activity (8). It is plausible that a similar effect is occurring in the salt-activated SC systems and that the presence of plasticizing residual water facilitates slower, larger-scale motions critical to catalysis. Although previous structural studies of SC in the aqueous phase tend to emphasize the importance of electrostatics over dynamic contributions to catalysis, it is beginning to appear that dynamics indeed play a larger role in proteolytic activity than was previously thought. In all, these results lend strong credence to the supposition that faster enzyme dynamics play a principal role in the activation of enzymes in organic solvents.

Experimental Methods

Materials. SC (from *Bacillus licheniformis*), *N*-acetyl phenylalanine ethyl ester, *N*-succinyl-Ala-Ala-Ala-*p*-nitroanilide (SAAPFpNA), 4-fluorobenzene sulfonyl chloride (4-FBSCl), and nonadecane were obtained from Sigma, and ESL was purchased from Toronto Research Chemicals. Deuterated *n*-hexane (98.0%) was

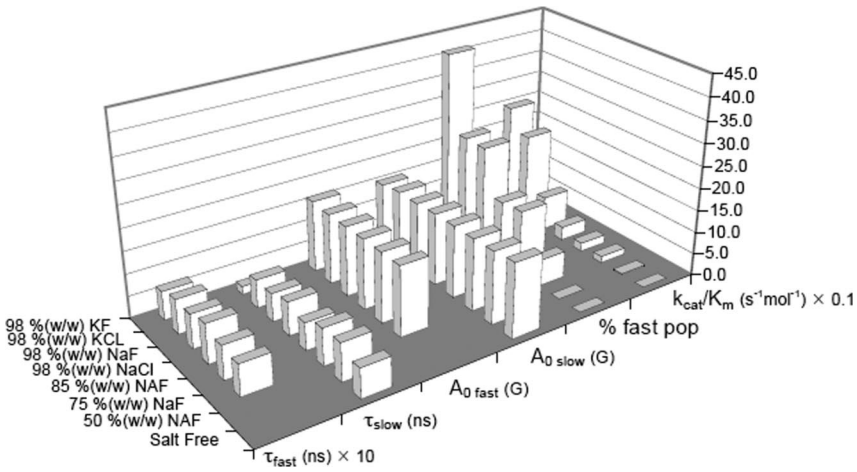

Fig. 7. ESR simulation parameters for SC biocatalysts.

obtained from Cambridge Isotope Laboratories. All solvents and salts used were of the highest grade commercially available, and the solvents were stored over molecular sieves (0.3 nm Linde) for at least 48 h before use.

Enzyme Preparation. The lyophilized biocatalyst sample was prepared by using a two-step protocol. Fifty-milliliter Falcon tubes containing specified aqueous mixtures of enzyme and salt in D_2O (pD 8.2) were vertically immersed in liquid N_2 for 2 min. Samples were then placed on Labconco Freeze Dry 6 freeze dryer (Fisher Scientific) at −49°C and 50 μm·Hg for 44 h. For enzyme samples containing salts, the phosphate buffer concentration of 0.25 mg/ml K_2HPO_4 and enzyme concentration of 0.25 mg/ml remained the same for all samples. The salt concentrations were adjusted to yield an ionic strength of I = 0.658 mol/kg D_2O. Salt-free enzyme (24.75 mg/ml) solutions in phosphate buffer, K_2HPO_4 (0.25 mg/ml, pD 8.2), were frozen and lyophilized in the same manner. The lyophilized samples were immediately assayed for activity and water content. The pD of all enzyme solutions was adjusted to 8.2 by using a few drops of 0.5 M KOH or 0.1 M H_3PO_4; in all cases the amount added did not significantly alter the buffer concentration, ionic strength, or solution volume. Samples were lyophilized from D_2O to spectrally edit ^{1}H NMR signals arising from residual water molecules associated with the biocatalyst.

Kinetic Assays. Catalytic efficiencies of subtilisin formulations were determined in anhydrous acetone and hexane. Transesterification of APEE with 1-propanol typically involved adding 5–10 mg of salt enzyme powder to 5 ml of organic solvent containing 1.5 mM nonadecane (internal standard for gas chromatography), 0.85 M 1-propanol, and various concentrations of APEE (1–20 mM). Reactions were carried out in 20-ml glass scintillation vials and agitated at 250 rpm in a C-24 Classic Benchtop Incubator Shaker (New Brunswick Scientific) at fixed temperature. Enthalpic and entropic contributions to catalysis were determined via variable temperature kinetic assays performed at 10°C, 15°C, 20°C, and 30°C. Thermodynamic properties were extracted by using an Eyring plot analysis with the equations below as detailed by Moore and Pearson (45), where κ is the preexponential transmission coefficient and the other parameters have their usual definitions.

$$\frac{k_{\rm cat}}{K_{\rm M}} = \kappa\left(\frac{k_{\rm B}T}{h}\right)\exp\left(\frac{\Delta S^*}{R}\right)\exp\left(-\frac{\Delta H^*}{RT}\right) \qquad [1]$$

$$(\Delta\Delta X^*)_{\rm biocatalyst} = (\Delta X^*)_{\rm salt\text{-}activated} - (\Delta X^*)_{\rm salt\text{-}free} \qquad [2]$$

The transesterification product, *N*-acetyl-L-phenylalanine propyl ester, was monitored by using gas chromatography. Kinetic and chromatography methods used to extract the kinetic efficiencies are detailed by Eppler *et al.* (33).

Fluorine Inhibitor Preparation. The fluorinated inhibitor 4-FBSF was prepared from 4-FBSCl as previously reported (46) with the exception that the final product was not distilled. Purity and structure of the synthesized inhibitor were determined via ^{1}H and ^{19}F NMR. Concentration of the synthesized inhibitor was determined by comparison of integrated intensities of the aromatic (−101.5 ppm) and sulfonyl fluorine (61.5 ppm) peaks. The synthetic route yielded a product that was ≈95% 4-FBSF.

Inhibition of subtilisin was performed in the following manner: 4 mg/ml enzyme was incubated for 2 h at a 1:1 stoichiometric ratio of enzyme to 4-FBSF in 20 mM bis-Tris-Propane 5% (vol/vol) acetone. Free inhibitor was removed by running the reaction solution through a YM-5 fixed-angle Amicon Centrifugal Filter at 4,000 × *g* for 45 min. The enzyme concentration was then determined by using a Bradford assay monitoring absorbance at 595 nm. To ensure that the enzyme remains inhibited throughout the filtration procedure, the enzyme activity was tested for hydrolysis of SAAPFpNA in 50 mM phosphate buffer. The inhibited biocatalyst was prepared as a lyophilized powder, as described above, and assayed in the organic phase to ensure continued inhibition throughout the freeze-drying process.

ESL Inhibition. Inhibition of subtilisin was performed following the procedure laid out by Morrisett and Broomfield (47) with the exception that acetonitrile rather than benzene was used as a cosolvent. Enzyme (23 mg/ml) was incubated for 5 min in a 1:5 stoichiometric ratio of enzyme to ESL in 100 mM sodium acetate buffer at pH 5.5 with 5% (vol/vol) acetonitrile. Labeled enzyme was then separated from free spin label and tested for activity as described in the preceding section.

^{19}F NMR. Fluorine experiments were performed on a Tecmag Apollo spectrometer at 7.39 Tesla (282.231 MHz). Inhibited biocatalyst ^{19}F chemical shift measurements were performed by using a using Hahn echo pulse sequence (90-τ to 180-τ-acq) with a delay of τ = 500 μs. The echo experiments were performed with a 90° pulse width of 12 μs, spectral width of 500 kHz, 2,096 real data points, and a recycle delay of 1.5 s. The number of scans ranged from 30,000 to 50,000. Typical experiments were performed as follows: a biocatalyst sample (20 mg/ml) was placed in a 10-mm NMR tube containing hexane and allowed to equilibrate for 1 h. The NMR tube was then placed in the magnet for spectral analysis.

^{1}H NMR. Proton relaxation experiments were performed on a home-built spectrometer at 9.39 Tesla (400.00134 MHz). In a typical experiment, 50–75 mg of sample (biocatalyst) was packed into a 3.2-mm (36-μl) Varian rotor under N_2 to avoid adsorption of ambient H_2O. A small amount of deuterated hexane was then added to the rotor (≈15 μl), and the sample was allowed to equilibrate for 1 h. The rotor was then placed in a T3 Varian Solids NMR probe, and proton relaxation times were recorded. Relaxation data presented in this study represent

Table 1. ESR simulation parameters for SC biocatalysts

Conditions	k_{cat}/K_m, $s^{-1}\cdot M^{-1}$	% faster population	$\tau_{c\ fast}$, $\tau_{c\ slow}$, ns	A_0, G
Salt-free	0.092	—	—, 6.61	—, 16.8
50% (wt/wt) NaF	2.12	—	—, 8.51	—, 16.4
75% (wt/wt) NaF	14.5	0.06	0.71, 8.32	15.9, 16.3
85% (wt/wt) NaF	19.0	0.15	0.76, 6.22	15.9, 16.4
98% (wt/wt) NaCl	30.5	0.14	0.89, 7.59	15.9, 16.3
98% (wt/wt) NaF	76.8	0.24	0.78, 6.35	15.9, 16.1
98% (wt/wt) KCl	200	0.24	0.78, 6.37	15.9, 16.1
98% (wt/wt) KF	248	0.41	0.64, 1.86	16.2, 15.3

overall proton dynamics within the enzyme/biocatalyst. Spectra were recorded with magic angle spinning speeds in the range of 15 kHz, stable within ± 10 Hz, and all delays were rotor-synchronized. Activity assays of the biocatalyst after exposure to the high spinning rates ensured that the centrifugal forces exerted during the MAS experiment did not significantly affect the structure of the biocatalysts.

Three NMR relaxation experiments were chosen to investigate enzyme dynamics within the biocatalyst formulation. NMR relaxation times are quantitatively related to molecular motion because the fluctuating magnetic fields associated with spin motions induce nuclear spin transitions. The rates of these transitions, or their corresponding relaxation times, are measured according to well known protocols (22–24). Spin-lattice relaxation, T_{1H}, was measured via saturation recover to assess global enzyme dynamics on a fast timescale, 1 ps to 10 ns. Intermediate enzyme dynamics on the 100-μs to 1-ms timescale were probed via spin-lattice relaxation in the rotating frame, $T_{1\rho H}$, using a B_{1rf} amplitude of 31.25 kHz. Slow dynamic timescales, 100 ms to 1 s, were measured by using double quantum protocols (e.g., by using longitudinal magnetization exchange experiments, T_{1zzH}) (22, 24). Each of these protocols was selected based on its sensitivity to spin transitions in the appropriate frequency range. For the particular case of protons associated with an enzyme suspension, nuclear spin relaxation is dominated by motion-induced fluctuations of the homonuclear dipole–dipole interaction. Within this model the relaxation times T_{1H}, $T_{1\rho H}$, and T_{1zzH} are nonlinear functions of the motional correlation time, τ_c, as shown below, where ω_I is the Larmor frequency, ω_{RF} is the lock frequency, and β is the lock angle (22–24).

$$\frac{1}{T_{1H}}=\frac{2}{3}I(I+1)\frac{\gamma_I^4\hbar^2}{r^6}\left\{\frac{\tau_c}{1+(\omega_{I\tau_c})^2}+\frac{4\tau_c}{1+(\omega_I\tau_c)^2}\right\} \quad [3]$$

$$\frac{1}{T_{1\rho H}}=\frac{1}{3}I(I+1)\frac{\gamma_I^4\hbar^2}{r^6}\left\{\begin{array}{l}3\sin^2\beta\cos^2\beta\dfrac{\tau_c}{1+(\omega_{RF}\tau_c)^2}+3\sin^4\beta\dfrac{\tau_c}{1+(2\omega_{RF}\tau_c)^2}\\+(5-3\cos^2\beta)\dfrac{\tau_c}{1+(\omega_I\tau_c)^2}+(6\cos^2\beta+2)\dfrac{\tau_c}{1+(2\omega_I\tau_c)^2}\end{array}\right\} \quad [4]$$

$$\frac{1}{T_{1zzH}}=\frac{1}{9}I(I+1)\frac{\gamma_I^4\hbar^2}{r^6}\left\{5\frac{\tau_c}{1+(0\times\tau_c)^2}+9\frac{\tau_c}{1+(\omega_I\tau_c)^2}+6\frac{\tau_c}{1+(2\omega_I\tau_c)^2}\right\} \quad [5]$$

Experimental and Simulated ESR Studies. ESR experiments were performed on a Bruker ER200D-SRC spectrometer at 298K. A typical spectrum was recorded as follows: 5–10 mg of inhibited biocatalyst was suspended in 1 ml of solvent, sonicated for 30 s, and placed in the spectrometer. Spectra were recorded by using a microwave power of 1.26 mW, modulation amplitude of 2 G, and a sweep width of 150 G.

Spectral parameters were extracted from the experimental ESR spectra using the EasySpin software package (48) assuming a two-population model. The diffusional tensor D_i [$D_i = 1/(6\tau_i)$] and the hyperfine splitting constant A_0 were allowed to vary, and least-squares analysis was used to fit the simulations to the data. Variation of the simulation starting parameters ensured robustness of fit.

ACKNOWLEDGMENTS. This work was supported by National Science Foundation Grant BES-0228145 and National Institutes of Health Grant GM66712.

1. Henzler-Wildman KA, Kern D (2007) Dynamic personalities of proteins. *Nature* 450:964–972.
2. Schnell JR, Dyson HJ, Wright PE (2004) Structure, dynamics, and catalytic function of dihydrofolate reductase. *Annu Rev Biophys Biomol Struct* 33:119–140.
3. Benkovic SJ, Hammes-Schiffer S (2003) A perspective on enzyme catalysis. *Science* 301:1196–1202.
4. Eisenmesser EZ, *et al*. (2005) Intrinsic dynamics of an enzyme underlies catalysis. *Nature* 438:117–121.
5. Henzler-Wildman KA, *et al*. (2007) Intrinsic motions along an enzymatic reaction trajectory. *Nature* 450:838–844.
6. McElheny D, Schnell JR, Lansing JC, Dyson HJ, Wright PE (2005) Defining the role of active-site loop fluctuations in dihydrofolate reductase catalysis. *Proc Natl Acad Sci USA* 102:5032–5037.
7. Kovrigin EL, Loria JP (2006) Characterization of the transition state of function enzyme dynamics. *J Am Chem Soc* 128:7724–7725.
8. Sola RJ, Griebenow K (2006) Chemical glycosylation: New insights on the interrelation between protein structural mobility, thermodynamic stability, and catalysis. *FEBS Lett* 580:1685–1690.
9. Castillo B, Solá RJ, Ferrer A, Barletta G, Griebenow K (2008) Effect of PEG modification on subtilisin Carlsberg activity, enantioselectivity, and structural dynamics in 1,4-dioxane. *Biotechnol Bioeng* 99:9–17.
10. Klibanov AM (2001) Improving enzymes by using them in organic solvents. *Nature* 409:241–246.
11. Clark DS (2004) Characteristics of nearly dry enzymes in organic solvents: Implications for biocatalysis in the absence of water. *Philos Trans R Soc London B* 359:1299–1307.
12. Halling PJ (2004) What can we learn by studying enzymes in non-aqueous media? *Philos Trans R Soc London B* 359:1287–1297.
13. Schmid A, *et al*. (2001) Industrial biocatalysis today and tomorrow. *Nature* 409:258–268.
14. Paradkar VM, Dordick JS (1994) Aqueous-like activity of alpha-chymotrypsin dissolved in nearly anhydrous organic solvents. *J Am Chem Soc* 116:5009–5010.
15. Griebenow K, Vidal M, Baéz C, Santos AM, Barletta G (2001) Native-like enzyme properties are important for optimum activity in neat organic solvents. *J Am Chem Soc* 123:5380–5381.
16. Griebenow K, *et al*. (1999) Improved enzyme activity and enantioselectivity in organic solvents by methyl-β-cyclodextrin. *J Am Chem Soc* 121:8157.
17. Ru MT, *et al*. (2000) On the salt-induced activation of lyophilized enzymes in organic solvents: Effect of salt kosmotropicity on enzyme activity. *J Am Chem Soc* 122:1565–1571.
18. Lindsay JP, Clark DS, Dordick JS (2004) Combinatorial formulation of biocatalyst preparations for increased activity in organic solvents: Salt activation of penicillin amidase. *Biotechnol Bioeng* 85:553–560.
19. Burke PA, Griffin RG, Klibanov AM (1993) Solid-state nuclear magnetic resonance investigation of solvent dependence of tyrosyl ring motion in an enzyme. *Biotechnol Bioeng* 42:87–94.
20. Affleck R, Haynes CA, Clark DS (1992) Solvent dielectric effects on protein dynamics. *Proc Natl Acad Sci USA* 89:5167–5170.
21. Broos J, *et al*. (1995) Flexibility of enzymes suspended in organic solvents probed by time-resolved fluorescence anisotropy. Evidence that enzyme activity and enantioselectivity are directly related to enzyme flexibility. *J Am Chem Soc* 117:12657–12663.
22. Levitt MH (2008) in *Spin Dynamics* (Wiley, Hoboken, NJ), pp 509–595.
23. Mehring M (1983) in *Principles of High Resolution of NMR in Solids* (Springer, New York), pp 260–287.
24. Millet O, Muhandiram DR, Skrynnikov NR, Kay LE (2002) Deuterium spin probes of side-chain dynamics in proteins. 1. Measurement of five relaxation rates per deuteron in (13)C-labeled and fractionally (2)H-enriched proteins in solution. *J Am Chem Soc* 124:6439–6448.
25. Dabulis K, Klibanov AM (1993) Dramatic enhancement of enzymatic activity in organic solvents by lyoprotectants. *Biotechnol Bioeng* 41:566–571.
26. Triantafyllou AO, Wehtje E, Adlercreutz P, Mattiasson B (1996) How do additives affect enzyme activity and stability in nonaqueous media? *Biotechnol Bioeng* 54:67–76.
27. Burke PA, Griffin RG, Klibanov AM (1992) Solid-state NMR assessment of enzyme active center structure under nonaqueous conditions. *J Biol Chem* 267:20057–20064.
28. Chang BS, Randall CS (1992) Use of sub-ambient thermal analysis to optimize protein lyophilization. *Cryobiology* 29:632–656.
29. Reif B, *et al*. (2006) Protein side-chain dynamics observed by solution- and solid-state NMR: Comparative analysis of methyl 2H relaxation data. *J Am Chem Soc* 128:12354–12355.
30. Hologne M, Faelber K, Diehl A, Reif B (2005) Characterization of dynamics of perdeuterated proteins by MAS solid-state NMR. *J Am Chem Soc* 127:11208–11209.
31. McDermott A (2004) Structural and dynamic studies of proteins by solid-state NMR spectroscopy: Rapid movement forward. *Curr Opin Struct Biol* 14:554–561.
32. Lee CS, *et al*. (1998) Multinuclear NMR study of enzyme hydration in an organic solvent. *Bioeng Biotechnol* 57:686–693.
33. Eppler RK, *et al*. (2006) Water dynamics and salt-activation of enzymes in organic media: Mechanistic implications revealed by NMR spectroscopy. *Proc Natl Acad Sci USA* 103:5706–5710.
34. Fenimore P, Frauenfelder H, McMahon B, Parak F (2002) Slaving: Solvent fluctuations dominate protein dynamics and functions. *Proc Natl Acad Sci USA* 99:16047–16051.
35. Kamal JKA, Zhao L, Zewail AH (2004) Ultrafast hydration dynamics in protein unfolding: Human serum albumin. *Proc Natl Acad Sci USA* 101:13411–13416.
36. Frauenfelder H, Fenimore PW, Chen G, McMahon B (2006) Protein folding is slaved to solvent motions. *Proc Natl Acad Sci USA* 103:15469–15472.
37. Kamal A, *et al*. (2004) Enzyme functionality and solvation of subtilisin Carlsberg: From hours to femtoseconds. *Chem Phys Lett* 387:209–215.
38. Pal SK, Peon J, Zewail AH (2002) Ultrafast surface hydration dynamics and expression of protein functionality: α-Chymotrypsin. *Proc Natl Acad Sci USA* 99:15297–15302.
39. Daniel RM, *et al*. (1998) Enzyme activity below the dynamical transition at 220 K. *Biophys J* 75:2504–2507.
40. Dunn RV, *et al*. (2000) Enzyme activity and dynamics: Xylanase activity in the absence of fast anharmonic dynamics. *Biochem J* 346:355–358.
41. Angle CD, Oldfield E (1994) Evaluating ^{19}F chemical shielding in fluorobenzenes: Implications for chemical shifts in proteins. *J Am Chem Soc* 116:7453–7454.
42. Affleck R, *et al*. (1992) Enzymatic catalysis and dynamics in low-water environments. *Proc Natl Acad Sci USA* 89:1100–1104.
43. Suzawa VM, *et al*. (1995) Suspended and immobilized chymotrypsin in organic media: Structure-function relationships revealed by ESR spectroscopy. *J Am Chem Soc* 117:8435–8440.
44. Carnevale V, Raugei S, Micheletti C, Carloni P (2006) Convergent dynamics in the protease enzymatic superfamily. *J Am Chem Soc* 128:9766–9772.
45. Moore JW, Pearson RG (1981). *Kinetics and Mechanism* (Wiley, New York).
46. Gerig JT, Roe DC (1974) Kinetics of Inactivation of alpha-chymotrypsin with substituted benzenesulfonyl fluorides. *J Am Chem Soc* 96:233–238.
47. Morrisett JD, Broomfield CA (1972) Comparative study of spin-labeled serine enzymes—acetylcholinesterase, trypsin, alpha-chymotrypsin, elastase, and subtilisin. *J Biol Chem* 247:7224–7231.
48. Stoll S, Schweiger A (2006) EasySpin, a comprehensive software package for spectral simulation and analysis of EPR. *J Magn Reson* 178:42–55.